Applied Surface Science 393 (2017) 134–143

Contents lists available at ScienceDirect

Applied Surface Science

journal homepage: www.elsevier.com/locate/apsusc

Full Length Article

Effect of synthesis route on electrical and ethanol sensing characteristics for $LaFeO_{3-\delta}$ nanoparticles by citric sol-gel method

Ensi Cao *[,1], Yuqing Yang [1], Tingting Cui, Yongjia Zhang, Wentao Hao, Li Sun, Hua Peng, Xiao Deng

Key Lab. of Advanced Transducers & Intelligent Control System, College of Physics & Optoelectronics, Taiyuan University of Technology, Taiyuan 030024, People's Republic of China

ARTICLE INFO

Article history:
Received 27 June 2016
Received in revised form 3 October 2016
Accepted 3 October 2016
Available online 5 October 2016

Keywords:
$LaFeO_3$
Sol-gel
XPS
Ethanol sensing
Gas sensor

ABSTRACT

$LaFeO_{3-\delta}$ nanoparticles were prepared by citric sol-gel method with different raw material choosing and calcination process. The choosing of polyethylene glycol instead of ethylene glycol as raw material and additional pre-calcination at 400 °C rather than direct calcination at 600 °C could result in the decrease of resistance due to the reduction of activation energy Ea. Meanwhile, the choosing of ethylene glycol as raw material and additional pre-calcination leads to the enhancement of sensitivity to ethanol. Comprehensive analysis on the sensitivity and XRD, SEM, TEM, XPS results indicates that the sensing performance of $LaFeO_{3-\delta}$ should be mainly determined by the adsorbed oxygen species on Fe ions, with certain contribution from native active oxygen. The best sensitivity of 46.1–200 ppm ethanol at prime working temperature of 112 °C is obtained by the sample using ethylene glycol as raw material with additional pre-calcination, which originates from its uniformly-sized and well-dispersed particles as well as high atomic ratio of Fe/La at surface region.

1. Introduction

Gas sensors based on $LaFeO_3$ nanoparticles have attracted considerable interests due to their high sensitivity and stability to ethanol and tunable selectivity to various gases by the substitution of cation ions [1–17]. Among various methods that can be used to prepare $LaFeO_3$ nanoparticles, sol-gel method using citric acid has been frequently adopted due to the lost cost of raw materials and easy handle of procedures.

Aside from the common use of lanthanum nitrate, iron nitrate and citric acid in sol-gel method for the preparation of $LaFeO_3$ nanoparticles, polyethylene glycol (PEG) or ethylene glycol (EG) is also incorporated into the precursor solution by some researchers, and the gas sensing performance differs greatly from each other. Shi et al. prepared Ca-doped $LaFeO_3$ powders using PEG as raw material, and the $La_{0.8}Ca_{0.2}FeO_3$ shows good sensing performance towards CO at 180 °C [10]. Murade et al. prepared Sr-doped nanostructured $LaFeO_3$ using EG as raw material, and the nanocrystalline $La_{0.7}Sr_{0.3}FeO_3$ exhibited good sensing performance towards acetone at 275 °C [18]. Although the effect of dopant element and doping concentration on the gas sensing properties of $LaFeO_3$ has been investigated frequently, the comparative study on the effect of raw material choosing of PEG and EG has not been conducted so far. Besides direct calcination of the dry gel at high temperature, the final product of $LaFeO_{3-\delta}$ nanoparticles was obtained by some investigators with additional pre-calcination at low temperature, and shows different gas sensing performance. Chen et al. prepared $LaFeO_3$ nanocrystalline powders using PEG with pre-calcination at 400 °C for 2 h, and the final product annealed at 800 °C for 4 h can sensitively detect low concentration of acetone at 260 °C [19]. While nonstoichiometric $LaFeO_3$ powders prepared by Cao et al. using PEG through direct calcination at 600 °C for 2 h exhibited good sensitivity and selectivity towards ethanol at 140 °C [20]. Therefore, the gas sensing performance of $LaFeO_3$ nanoparticles depends not only on the raw material choosing, but also on the calcination process, and it is necessary to investigate the effect of synthesis route on the gas sensing characteristics of $LaFeO_3$ nanoparticles by citric sol-gel method.

When exploring the gas sensing mechanism of $LaFeO_3$-based sensors, the high sensitivity of $LaFeO_3$ nanoparticles to ethanol has always been ascribed to small crystallite size and large amount of adsorbed oxygen species (O_2^- or O^-) [5,10], which is supported by the relevance of sensitivity and the relative content of the

* Corresponding author.
E-mail address: caoensi@163.com (E. Cao).
[1] These authors contributed equally to this paper.

http://dx.doi.org/10.1016/j.apsusc.2016.10.013
0169-4332/

Table 1
Preparation differences for different $LaFeO_{3-\delta}$ samples.

Sample	EG	PEG	Pre-calcined at 400 °C	Calcined at 600 °C
PEG600	No	Yes	No	Yes
PEG400+600	No	Yes	Yes	Yes
EG600	Yes	No	No	Yes
EG400+600	Yes	No	Yes	Yes

adsorbed oxygen in the total surface oxygen (O_{ads}/O_{total}) from surface-sensitive XPS analysis. However, oxygen adsorption could take place on La, Fe ions and adventitious carbon, the effect of adsorbed oxygen species on the sensitivity will be amplified by the ratio of O_{ads}/O_{total} and the influence of the surface composition should be considered.

In the present work, $LaFeO_{3-\delta}$ nanoparticles were prepared by citric sol-gel method. The effect of synthesis route, specifically the choosing of PEG or EG as raw material and pre-calcination, on the electrical and ethanol sensing characteristics of $LaFeO_{3-\delta}$ nanoparticles were investigated for the first time, and the reason for the improvement of sensitivity was analyzed by the consideration of surface morphology and surface composition.

2. Experimental

2.1. Preparation of powders

$LaFeO_{3-\delta}$ powders were synthesized by citric sol-gel method. Analytical grade $La(NO_3)_3{\cdot}6H_2O$, $Fe(NO_3)_3{\cdot}9H_2O$, citric acid (CA), polyethylene glycol (PEG6000) and ethylene glycol (EG) were employed as raw materials. Firstly, stoichiometric amount of $La(NO_3)_3{\cdot}6H_2O$ and $Fe(NO_3)_3{\cdot}9H_2O$ were dissolved in ion-free water under continuous stirring to get a homogeneous solution. Then CA in 2:1 molar ratio with respect to the metallic cations was added to the solution as a chelator, and the solution was adjusted to a PH value of 6.5–7.5 by adding ammonia. After that, PEG or EG in 2:1 molar ratio with respect to the metallic cations was added to the mixed solution under stirring at 80 °C, which was sufficient for the polycondensation to obtain the sol. When using PEG as raw material, the stirring time was 6 h to form wet gel, while it was 10 h when EG was adopted. Thereafter, gel pieces were formed through combustion process, and were ground to form fine powders. Finally, some of the fine powders were directly calcined at 600 °C for 2 h in an oven, while others were pre-calcined for 2 h, remilled for half an hour, and post-calcined at 600 °C for 2 h. As analyzed by Qiu et al. [21], the exothermic peak at 403 °C in the DTA curve confirms the burnout of organic contents, where ethylene glycol (EG) and other raw materials were adopted as in our work. Therefore, 400 °C was chosen as the pre-calcination temperature to eliminate the organic components. To sum up, four kinds of $LaFeO_{3-\delta}$ powders were synthesized, and the preparation differences were summarized in Table 1.

2.2. Characteristics of powders

X-ray diffraction patterns of the obtained $LaFeO_{3-\delta}$ powders were measured by X-ray diffractometer (D/max 2500, Rigaku Corporation, Japan) using Cu Kα radiation. Surface morphology was measured by field emission scanning electron microscope (JSM-6700F, JEOL Ltd., Japan) and transmission electron microscope (JEM-2010, JEOL Ltd, Japan). X-ray photoelectron spectroscopy (XPS) measurements for $LaFeO_{3-\delta}$ nanocrystalline powders were performed with monochromated Al Kα radiation using X-ray photoelectron spectrometer (ESCALAB 250, Thermo Electron Corporation, USA).

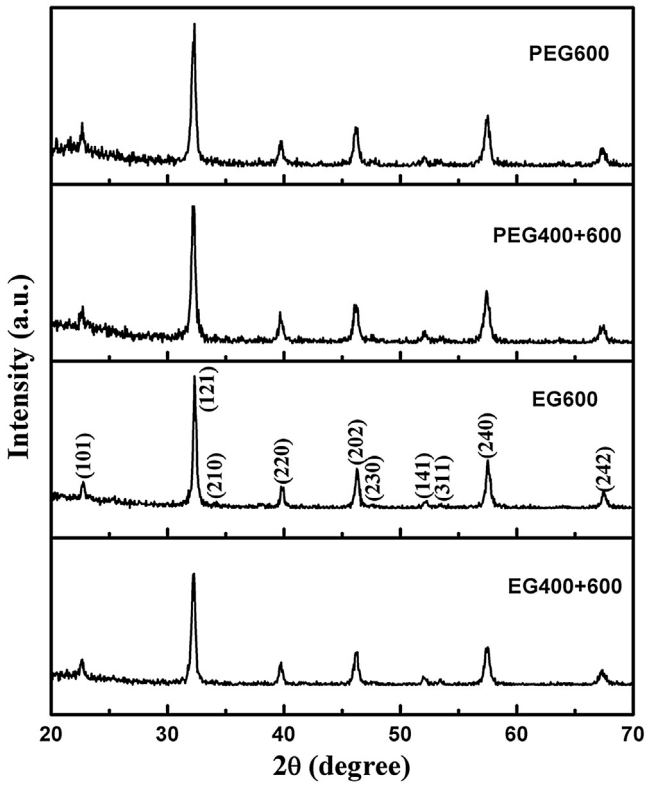

Fig. 1. X-ray diffraction patterns of different $LaFeO_{3-\delta}$ nanoparticles.

2.3. Fabrication and measurements of sensors

The details for the fabrication and measurement of sensors are described in our previous work [20]. The temperature of the sensor was controlled by the input current on the Ni-Cr heating wire (resistance = 35 Ω), and was measured by the contact of micro thermocouple on the outer surface of uncoated ceramic tube with Ni-Cr heating wire inside. Then a correlation between the input current and temperature was obtained and used as a criterion for subsequent determination of operating temperature. The operating temperature in our work refers to temperature on the outer surface of uncoated ceramic tube, and was varied between 96 and 200 °C. The sensor sensitivity was defined as the ratio (S = Rg/Ra) of the resistance of the sensor in target gases (Rg) and that in dry air (Ra). In order to make the measurement of sensitivity more precisely, in our present work, the gas desorption at 220 °C was introduced into each measuring procedure of sensitivity, because good reproducibility of resistance at 220 °C could be obtained before and after each measurement of sensitivity, and the influence of residual gas adsorption could be eliminated to great extent.

3. Results and discussion

3.1. Structural analysis

Fig. 1 shows the X-ray diffraction patterns of different $LaFeO_{3-\delta}$ nanoparticles. All the samples have a single phase with orthorhombic perovskite structure (space group Pnma-62), without any trace of impurity phase. Their lattice parameters, unit cell volumes, and average crystallite sizes are summarized in Table 2. The details for these calculations are described in our previous work [20].

The average crystallite size of PEG400+600 is 18.2 nm, which is slightly smaller than 18.9 nm of PEG600. Similarly, the average crystallite size is 23.6 nm for EG400+600, slightly smaller than

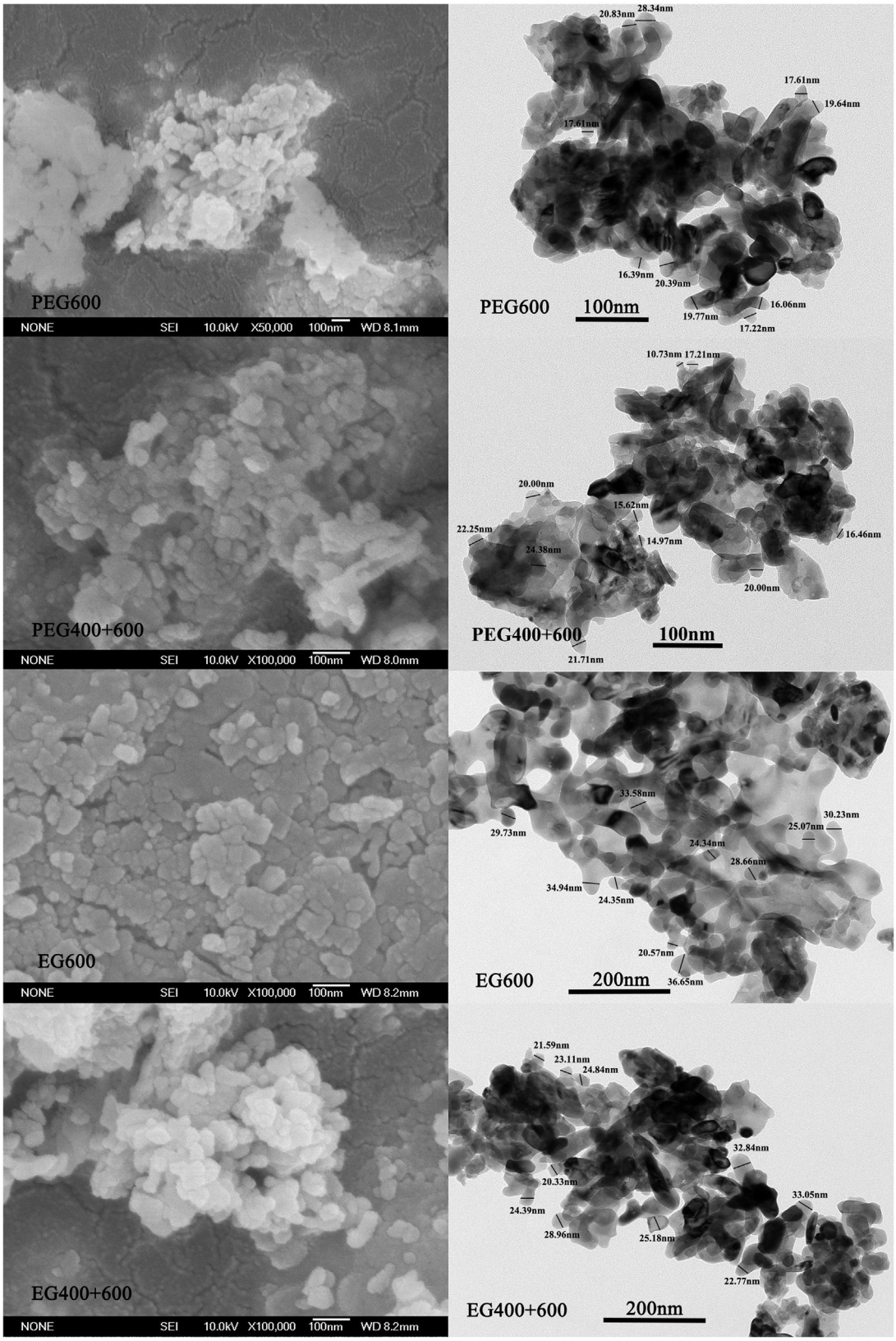

Fig. 2. SEM and TEM images of different $LaFeO_{3-\delta}$ nanoparticles.

24 nm of EG600. Considering the small change in crystallite size, the influence of additional pre-calcination on the crystallite size is not obvious by XRD, which will be explored by TEM below. However, it is obvious that the average crystallite size of the samples using PEG as raw material showed lower crystallite size than by using EG, because EG acts as bridge between CA-metal complexes and prevents the separation of components at later process stages [22], which would increase the degree of polymerization and facilitate

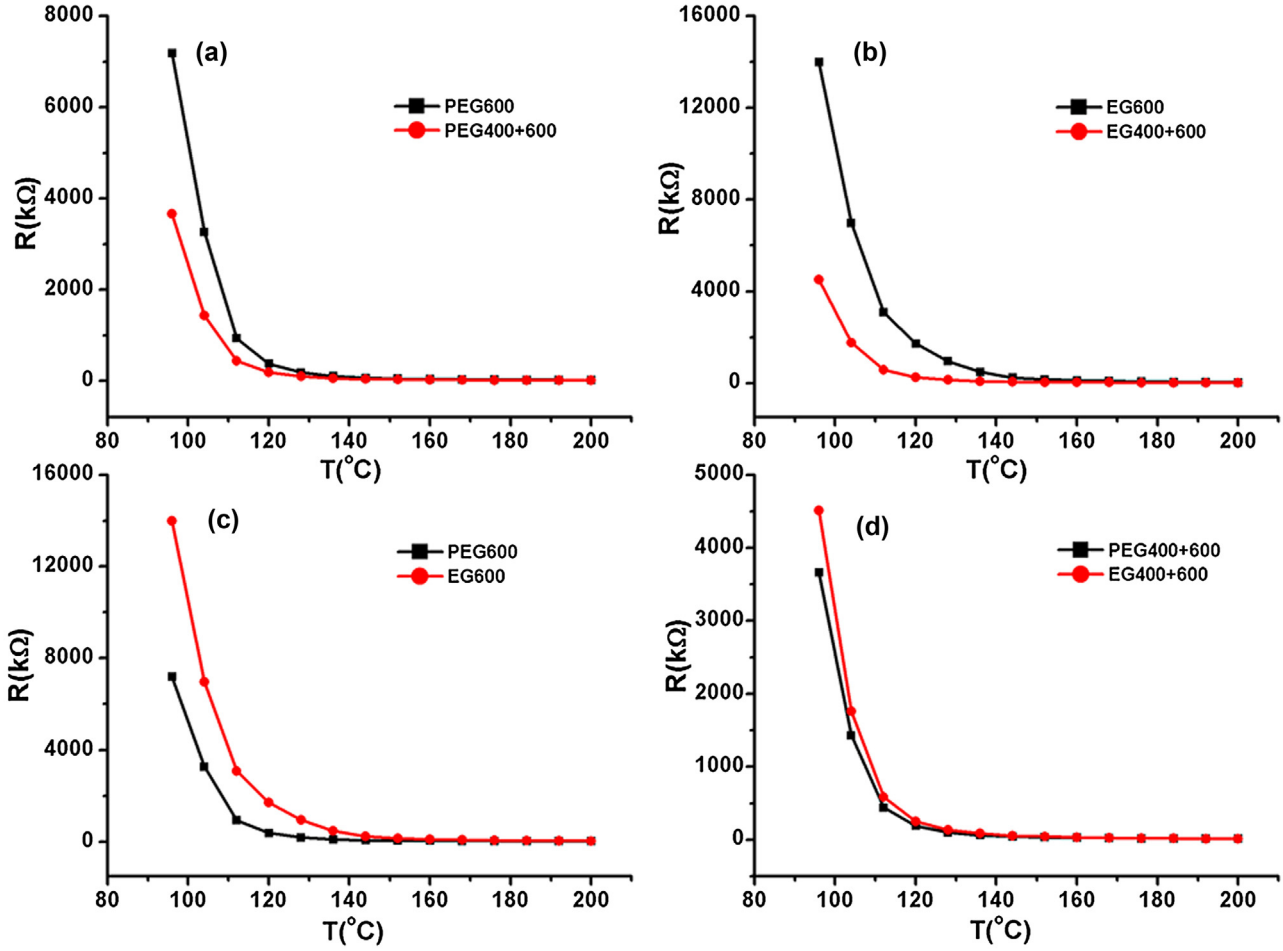

Fig. 3. Temperature dependence of resistances in air for different $LaFeO_{3-\delta}$ sensors in comparison.

Table 2
Lattice parameters, unit cell volume (V), average crystallite size (D), activation energy (Ea) for different $LaFeO_{3-\delta}$ samples.

Sample	a (Å)	b (Å)	c (Å)	V (Å^3)	D (nm)	Ea (eV)
PEG600	5.5632	7.8381	5.5476	241.90	18.9	0.45
PEG400+600	5.5560	7.8429	5.5549	242.06	18.2	0.42
EG600	5.5331	7.8285	5.5422	240.07	24.0	0.64
EG400+600	5.5591	7.8547	5.5521	242.43	23.6	0.50

the growth of crystallite. On the contrary, the non-ionic surfactant PEG acts as dispersant to improve the separation of CA-metal complex [23], which would decrease the degree of polymerization and inhibit the formation of big crystallite.

3.2. Surface morphology

Fig. 2 exhibits the SEM (left) and TEM (right) images of different $LaFeO_{3-\delta}$ nanoparticles. The particles are generally irregular and agglomerated, which in turn results in blurry outline of most particles. The specific size of ten small particles with relatively clear outline is indicated in the TEM images for each sample. Big particles are composed of smaller crystallites, and these selected small particles could be treated as crystallites. Thus the average crystallite size is 18.33 nm for PEG400+600, smaller than the 19.39 nm for PEG600. Likewise, the average crystallite size is 25.71 nm for EG400+600, smaller than the 28.81 nm for EG600. The TEM results are in good accordance with the XRD results. Although PEG results in smaller average crystallite size than EG, compared to PEG400+600, the particles of EG400+600 are more uniform in size and better dispersed. Thus the specific surface area is increased by EG, which makes the adsorption of ethanol more easily and the response enhanced. Different from EG400+600, the nanoparticles tend to agglomerate and coalesce in plane with direct calcination for EG600, leading to the formation of layered porous structure with large area. In other words, additional pre-calcination inhibits the coalescence of nanoparticles to some extent and results in smaller and better-dispersed particles when EG was adopted.

3.3. Electrical properties

The temperature dependence of resistances in air for different $LaFeO_{3-\delta}$ sensors in comparison is shown in Fig. 3. As seen in Fig. 3(a) and (b), the resistance of $LaFeO_{3-\delta}$ sensor with additional pre-calcination is smaller than that with direct calcination whether using PEG or EG as raw material at each fixed operating temperature. On the other side, as shown in Fig. 3(c) and (d), the resistance of $LaFeO_{3-\delta}$ sensor using PEG as raw material is smaller than that using EG as raw material, irrespective of additional pre-calcination. With the increase of temperature, the intrinsic resistivity of the material should monotonously decrease depending on its semiconducting nature, the influence of adsorbed oxygen species on the resistivity can be divided into three stages. From RT to prime working temperature, oxygen adsorption predominates and the adsorbed oxygen species (O^{2-} or O^-) capture more electrons from material, and contributes to the decrease of resistance. From prime working temperature above, oxygen desorption predominates and releases

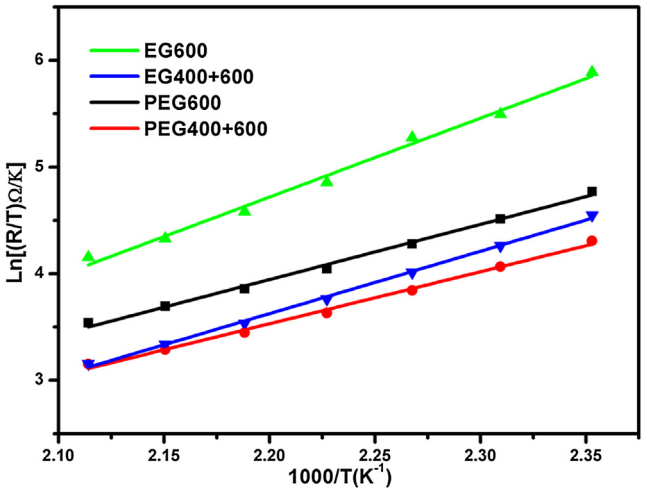

Fig. 4. ln[R/T] vs. 1000/T curve for different $LaFeO_{3-\delta}$ sensors.

electrons to the material, which leads to the increase of resistance. The resistance Ra measured at relatively lower temperature should be contributed from both the intrinsic nature of the material and adsorbed oxygen species. Only when the operating temperature is high enough for the complete desorption of oxygen species, the measured resistance of Ra reflects the intrinsic nature of the material.

Fig. 4 shows the ln[R/T] vs. 1000/T curve for different $LaFeO_{3-\delta}$ sensors in the measurement range of temperature from 152 °C to 200 °C, indicating that the intrinsic resistance R of all the samples fits best to Holsteins model of small polaron hopping conduction at relatively higher temperature [24–26]:

$$R(T) = R_0 T \exp(E_a/k_B T)$$

with $Ea = E_H + E_D/2$ for $T > \Theta_D/2$, and $Ea = E_D$ for $T < \Theta_D/4$, where E_a is activation energy, k_B is the Boltzmann constant, Θ_D is Deby temperature, E_H is the hopping energy and E_D is the disorder energy (the difference of electronic energies between two hopping sites). The obtained value of Ea for different $LaFeO_{3-\delta}$ sensors is displayed in Table 2. Similar to the case of average crystallite size, the Ea of the sample directly calcined at 600 °C is larger than that with additional pre-calcination at 400 °C, whether using PEG or EG as raw material. In addition, the Ea of the sample using PEG as raw material is smaller than that using EG as raw material, whether directly calcined at 600 °C or pre-calcined at 400 °C. Therefore, the reason that the choosing of PEG as raw material and additional pre-calcination result in the decrease of resistance is in essence due to the reduction of Ea, which makes the hopping of small polarons much easier.

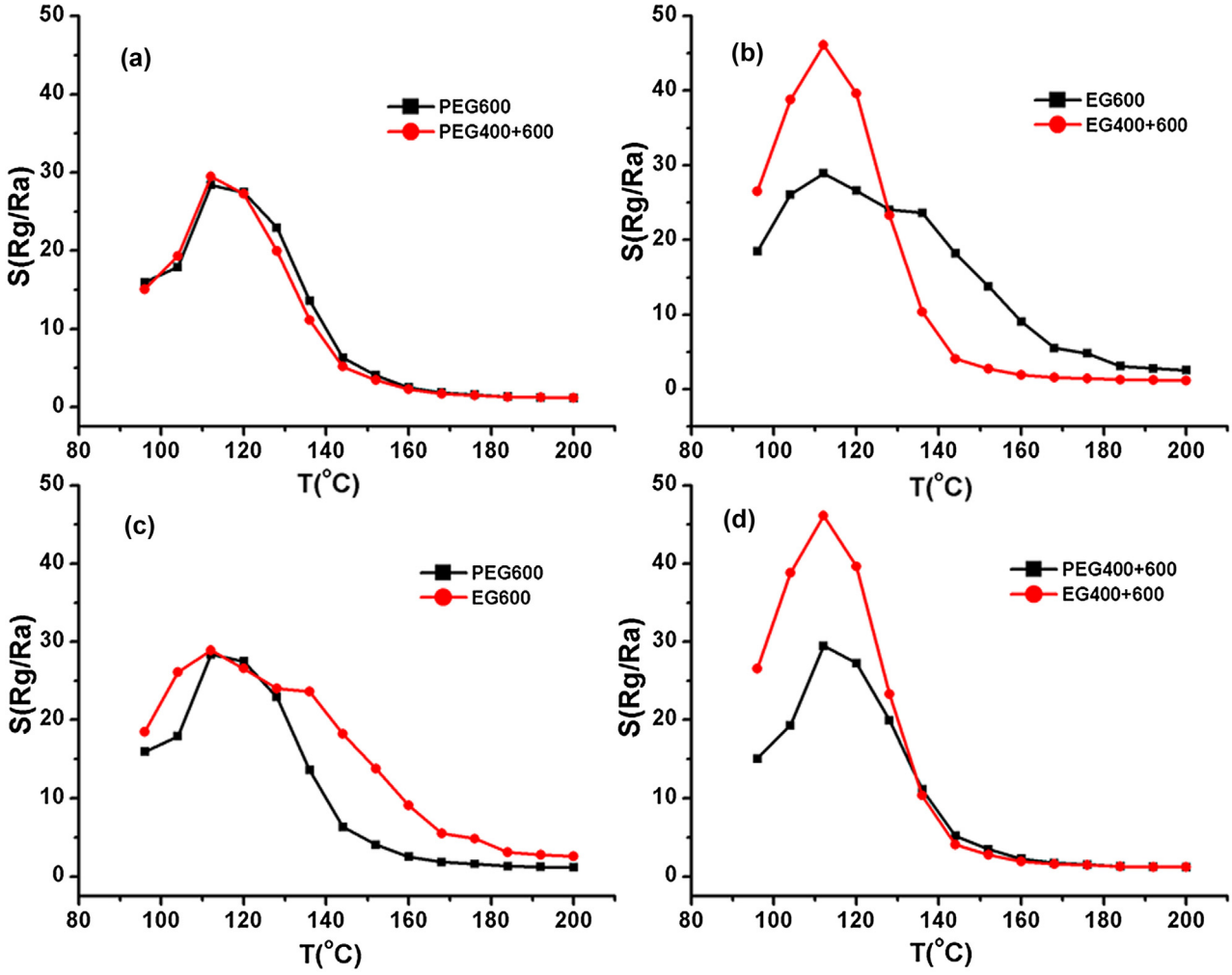

Fig. 5. Operating temperature dependence of sensitivity to 200 ppm ethanol for different $LaFeO_{3-\delta}$ sensors.

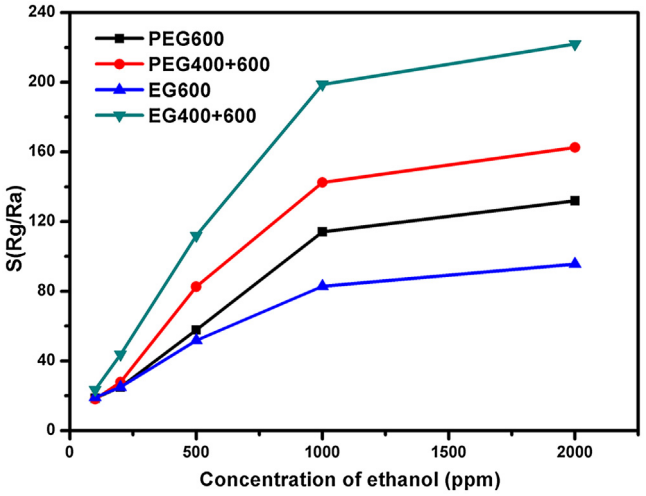

Fig. 6. Sensitivity of different $LaFeO_{3-\delta}$ sensors to different concentration of ethanol at prime working temperature of 112 °C.

3.4. Gas-sensing properties and mechanism

The operating temperature dependence of sensitivity to 200 ppm ethanol for different $LaFeO_{3-\delta}$ sensors in comparison is shown in Fig. 5. With increasing operating temperature, the sensitivity of all $LaFeO_{3-\delta}$ sensors increases at first, undergoes a maximum at 112 °C, and then decreases again. Therefore, 112 °C is considered as the prime working temperature for these sensors.

Table 3
Surface atomic concentrations (in %) and ratios of the different components for different $LaFeO_{3-\delta}$ samples.

Sample	La	Fe	O	C	Fe/La	Fe^{4+}/Fe^{3+}	O_{ads}/O_{total}	$C3/C_{total}$
PEG600	13.3	5.3	50.2	31.2	0.40	0.35	0.47	0.25
PEG400+600	13.6	5.8	52.4	28.2	0.43	0.32	0.47	0.26
EG600	13.2	6.7	51.4	28.7	0.51	0.30	0.36	0.20
EG400+600	13.4	7.5	51.1	28.0	0.56	0.31	0.37	0.20

As is known that the sensing response is due to the reaction between introduced ethanol and adsorbed oxygen species on the surface of sensing material, which results in the change of resistance of the sensor, oxygen from air can adsorb and desorb on the surface of particles and undergo the following reactions:

$$(a): O_{2(gas)} \leftrightarrow O_{2(ads)}$$

$$(b): O_{2(ads)} + e^- \leftrightarrow O_{2(ads)}^-$$

$$(c): O_{2(ads)}^- + e^- \leftrightarrow 2O_{ads}^-$$

$$(d): O_{ads}^- + e^- \leftrightarrow O_{ads}^{2-}$$

With the increase of operating temperature from room temperature, the equilibrium shifts to the right, and oxygen adsorption predominates. The adsorbed oxygen species (O_2^- or O^-) capture more electrons from $LaFeO_{3-\delta}$, and contributes to the decrease of resistance. However, further increase of temperature would make the equilibrium shift to the left and oxygen desorption predomi-

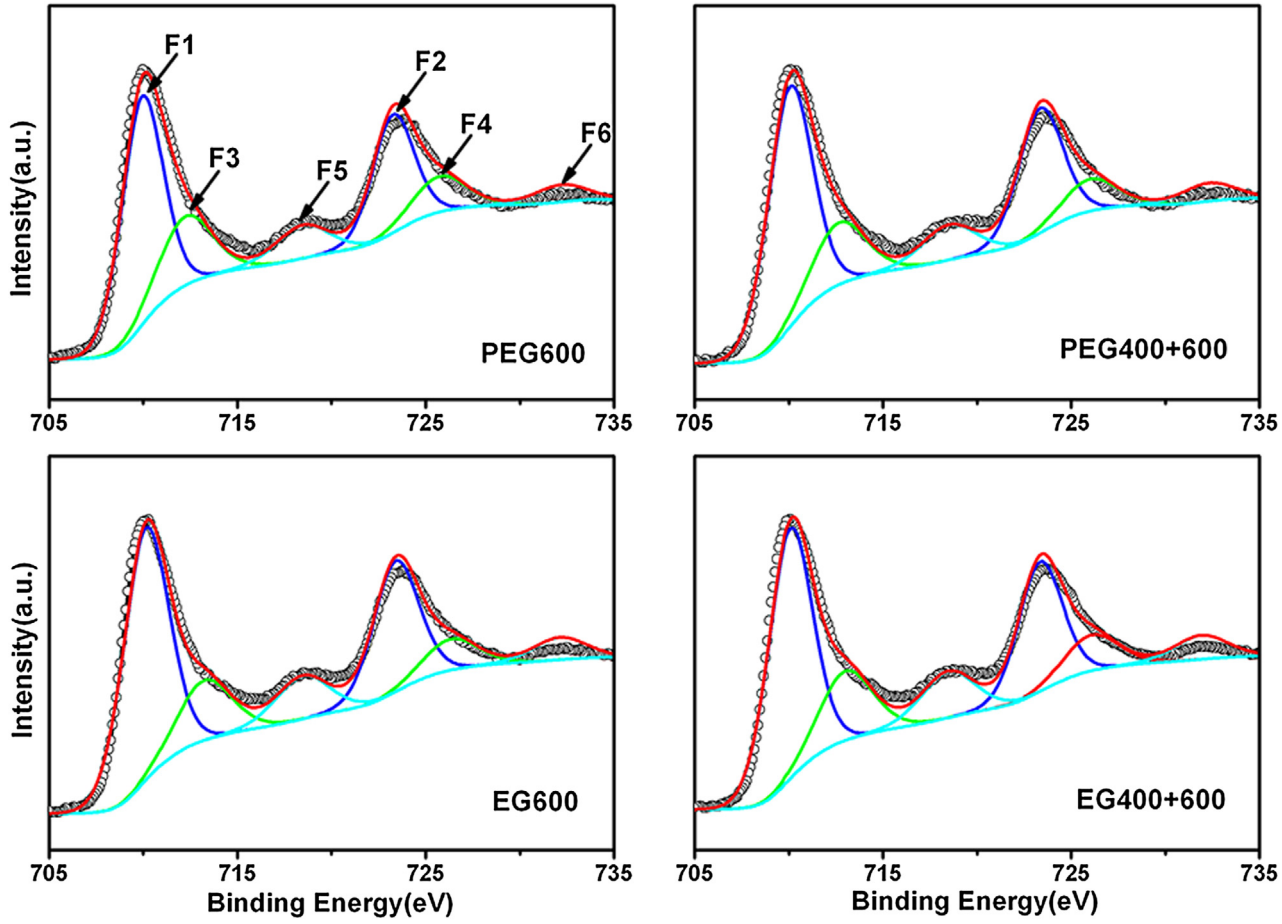

Fig. 7. The Fe2p XPS for different $LaFeO_{3-\delta}$ nanoparticles.

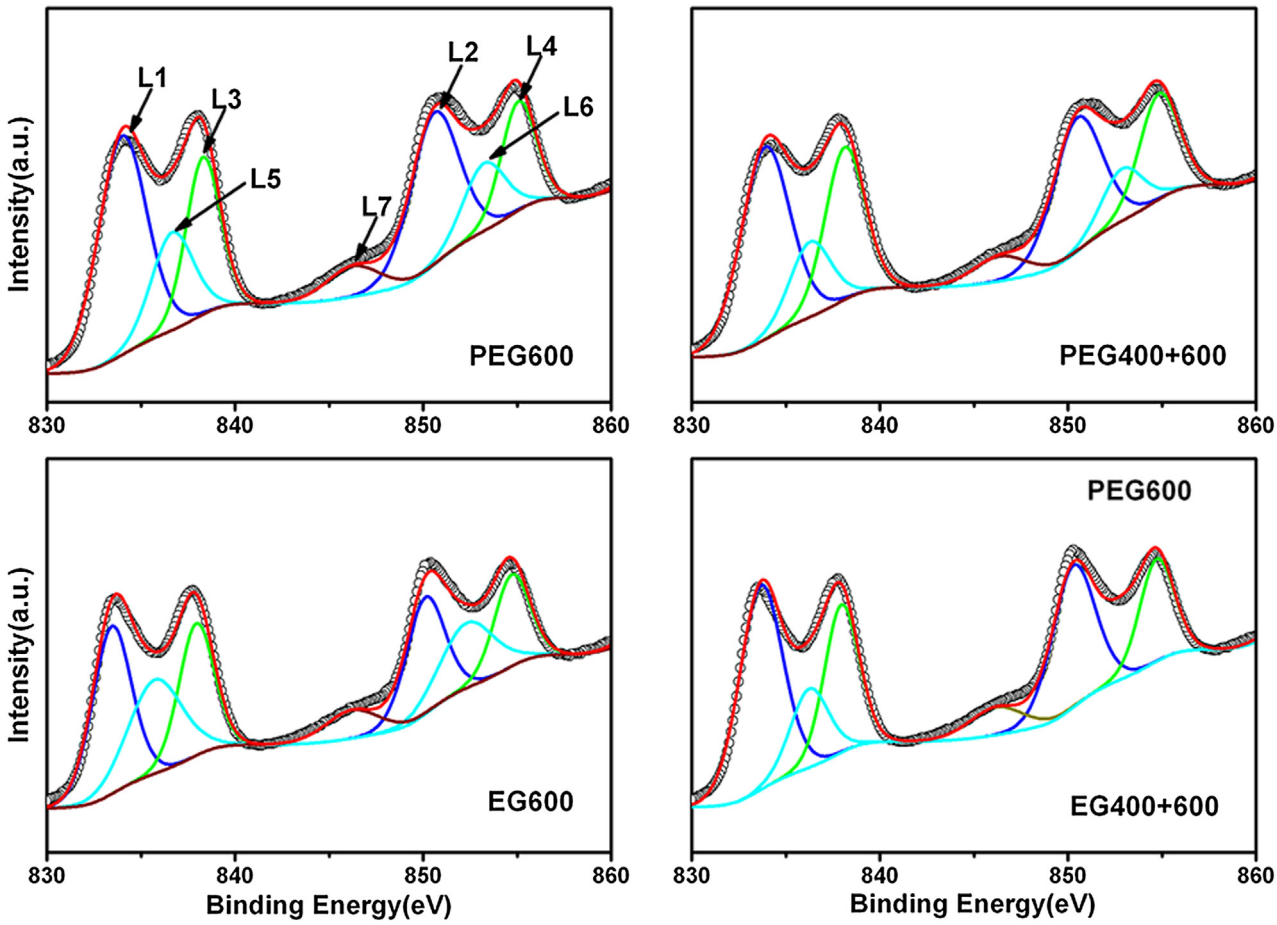

Fig. 8. The La3d XPS for different $LaFeO_{3-\delta}$ nanoparticles.

nates, which leads to the increase of resistance. As a consequence, a prime temperature exists, at which adsorbed oxygen species reach the maximum and prime sensitivity is obtained.

As shown in Fig. 5(a) and (b), additional pre-calcination did not make much difference to the sensitivity to 200 ppm ethanol over the measurement range of temperature when PEG was adopted, while great enhancement of sensitivity was observed from 90 to 120 °C when EG was used. Fig. 5(c) shows that the sensitivity of PEG600 and EG600 is close to each other at prime working temperature, while the sensitivity of EG400+600 is greatly enhanced around prime working temperature compared to PEG400+600, as shown in Fig. 5(d). Moreover, from Fig. 5(b) and (d), sharper increase and decline of sensitivity were observed below and above prime working temperature for EG400+600 than for EG600 and PEG400+600, indicating that the adsorption and desorption of oxygen are more convenient for EG400+600 due to its uniformly-sized and well-dispersed particles. The best sensitivity to 200 ppm ethanol is 46.1, which was obtained at 112 °C by EG400+600.

Fig. 6 displays the sensitivity of different $LaFeO_{3-\delta}$ sensors to different concentration of ethanol at prime working temperature of 112 °C. The sensitivity of each sensor increases fast with increasing concentration of ethanol in the range of 100–1000 ppm, while the increase rate becomes relatively slow from 1000 to 2000 ppm due to the limited active adsorption sites at the surface of each sensor. In addition, EG400+600 exhibits better response to ethanol than PEG400+600 at each fixed concentration, which is related to its larger specific area as analyzed by TEM. However, the sensitivity of EG600 to 500 ppm ethanol and above is lower than that of PEG600 due to its special layered porous structure with limited adsorption sites, which disfavors the adsorption of high concentration of ethanol on the surface of particles.

In our previous work, we have demonstrated that the ethanol sensing characteristics of $LaFeO_{3-\delta}$ sensors is greatly related with surface composition, hence the effect of synthesis route on the surface composition was checked by surface-sensitive XPS. Figs. 7 and 8 display the Fe2p and La3d XPS with peak deconvolutions for different $LaFeO_{3-\delta}$ nanoparticles, respectively. The results are similar to our previous work. For all the samples, Fe ions are in the mixed valence state of +3 (indicated by F1 and F2) and +4 (indicated by F3 and F4), La ions are present in the trivalent form. O1s and C1 s XPS with peak deconvolutions are displayed in Figs. 9 and 10, respectively, which verify the existance of adsorbed oxygen and mondentate La-carbonate La-O-CO_2 (indicated by O3 and C3) at the surface region.

Table 3 displays the surface atomic concentrations (in%) and ratios of the different components for different samples. The surface composition ratio is calculated according to the atomic concentration of each peak, which is calculated as: Normalized Peak Area × 100/Sum of Normalized Peak Areas. The Normalized Peak Area is calculated as: Peak Area/(SF × TXFN × ECF), where SF is sensitivity factor, TXFN is transmission function, and ECF is energy compensation factor. The calculation task was conducted with the help of Thermo Avantage (software). All samples exhibit La-rich surface, and the atomic ratio of Fe/La for PEG600 and PEG400+600 is 0.40 and 0.43 respectively, smaller than the corresponding values of 0.51 and 0.56 for EG600 and EG400+600. In other words, the choosing of EG as raw material and additional pre-calcination result in relatively higher concentration of Fe at the surface. Mean-

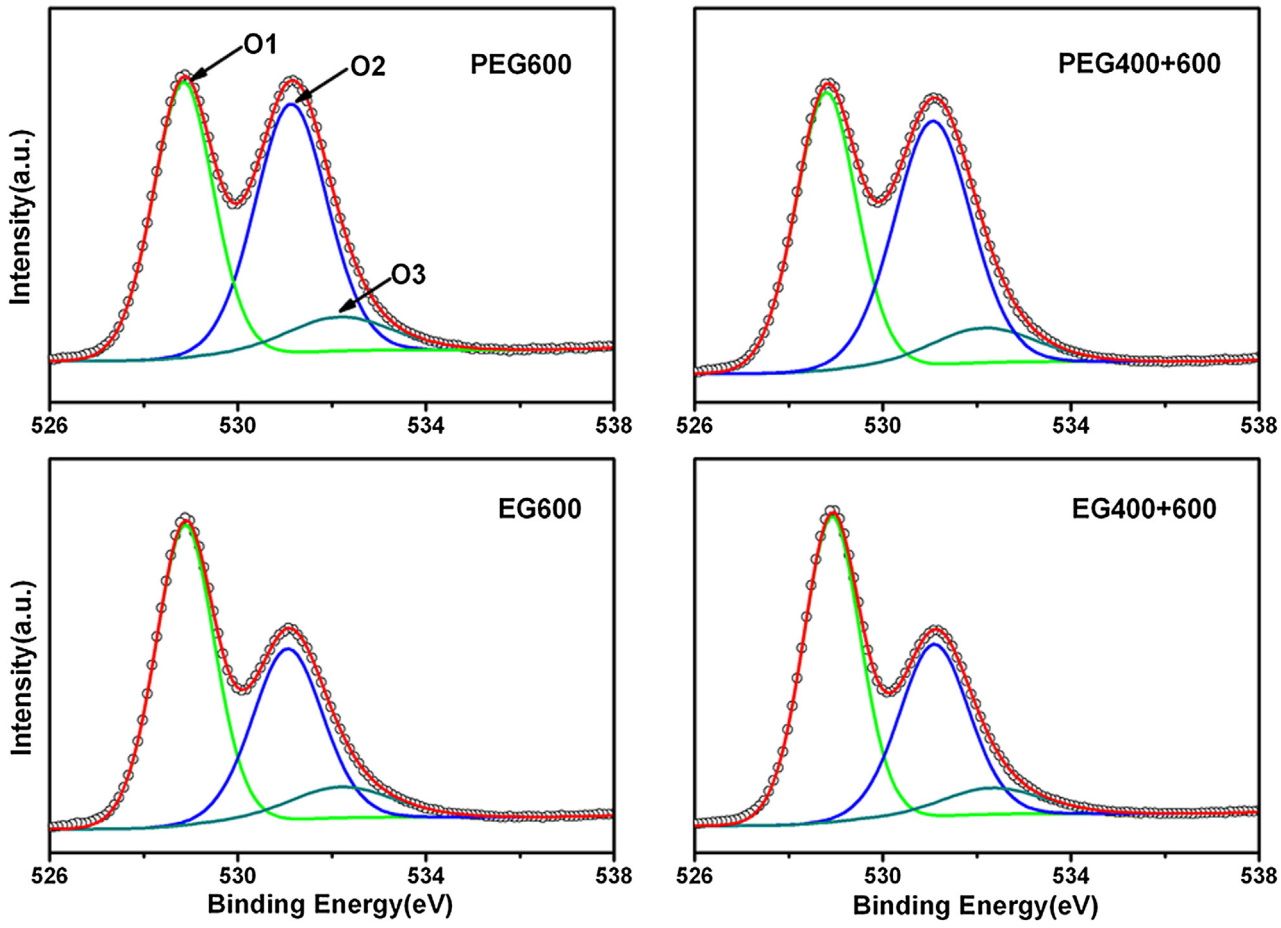

Fig. 9. The O1s XPS for different $LaFeO_{3-\delta}$ nanoparticles.

while, all the samples were prepared by stoichiometric amount of $La(NO_3)_3{\cdot}6H_2O$ and $Fe(NO_3)_3{\cdot}9H_2O$, therefore, La-rich surface means that La is poor inside the $LaFeO_3$ bulk beneath the surface, and relatively higher concentration of Fe at the surface would result in relatively higher concentration of La, namely, relatively less La vacancy inside the bulk.

The relative content of the adsorbed oxygen in the total surface oxygen (O_{ads}/O_{total}) for PEG600 is 0.47, which is identical with that for PEG400+600, and the ratio of O_{ads}/O_{total} for EG600 is 0.36, which is close with the value of 0.37 for EG400+600, indicating that the ratio of O_{ads}/O_{total} is related with the raw materials PEG and EG, and additional pre-calcination does not have too much influence on the ratio. On the other side, the ratio of O_{ads}/O_{total} for sample PEG600 and PEG400+600 is higher than that for sample EG600 and EG400+600, meaning that the choosing of PEG as raw material is beneficial for the increase of adsorbed oxygen on the surface of nanoparticles due to the relatively smaller particle size.

The case for the relative content of carbon in the form of La-O-CO_2 in the total surface carbon ($C3/C_{total}$) is similar to that for O_{ads}/O_{total}. Additional pre-calcination has little influence on the ratio of $C3/C_{total}$, and the choosing of PEG as raw material is beneficial for the formation of mondentate La-carbonate on the surface of nanoparticles which results in relatively higher ratio of La/Fe on the surface.

For ideally stoichiometric bulk $LaFeO_3$, all Fe ions belong to Fe^{3+}. However, in order to maintain the material to be charge neutrality, the La vacancies in $LaFeO_3$ lattice may induce Fe^{4+} or oxygen vacancy. When the sample was prepared under oxygen-rich atmosphere, oxygen vacancy compensation would be inhibited to some extent, and charge compensation would be dominant. Therefore, more La vacancy inside the bulk would facilitate the formation of Fe^{4+} ions. On the other side, according to *ab initio* calculation [27], the electron transfer from Fe ion to adsorbed oxygen could result in the transformation from Fe^{3+} to Fe^{4+} at some Fe site. On the whole, the formation of Fe^{4+} ions should be determined by oxygen adsorption on Fe ions at the surface region and by La vacancy inside the bulk due to charge compensation.

Since oxygen adsorption could take place on La ions and adventitious carbon besides Fe ions, only adsorbed oxygen species on Fe ions contribute to the formation of Fe^{4+} ions. Although there are more adsorbed oxygen species on the surface of PEG400+600, there are more Fe ions on the surface of EG400+600 as the atomic ratio of Fe/La is higher for EG400+600 than for PEG400+600, so the chance of oxygen adsorption on Fe ions is bigger for EG400+600 than for PEG400+600. In addition, compared to EG400+600, there are more La vacancies beneath the surface of PEG400+600, which favor the formation of Fe^{4+} ions due to charge compensation. The general effect is slightly higher atomic ratio Fe^{4+}/Fe^{3+} for PEG400+600 (0.32) than EG400+600 (0.31). Therefore, the higher sensitivity of EG400+600 than PEG 400 + 600 is related with its relatively higher atomic ratio of Fe/La.

Compared to PEG600, there are more adsorbed oxygen species on the surface Fe ions of PEG400+600, which contribute to the formation of Fe^{4+} ions. Meanwhile, there are less La vacancies beneath the surface of PEG400+600, which deteriorates the formation of Fe^{4+} ions from charge compensation. The general effect is little higher atomic ratio of Fe^{4+}/Fe^{3+} for PEG600 (0.35) than for

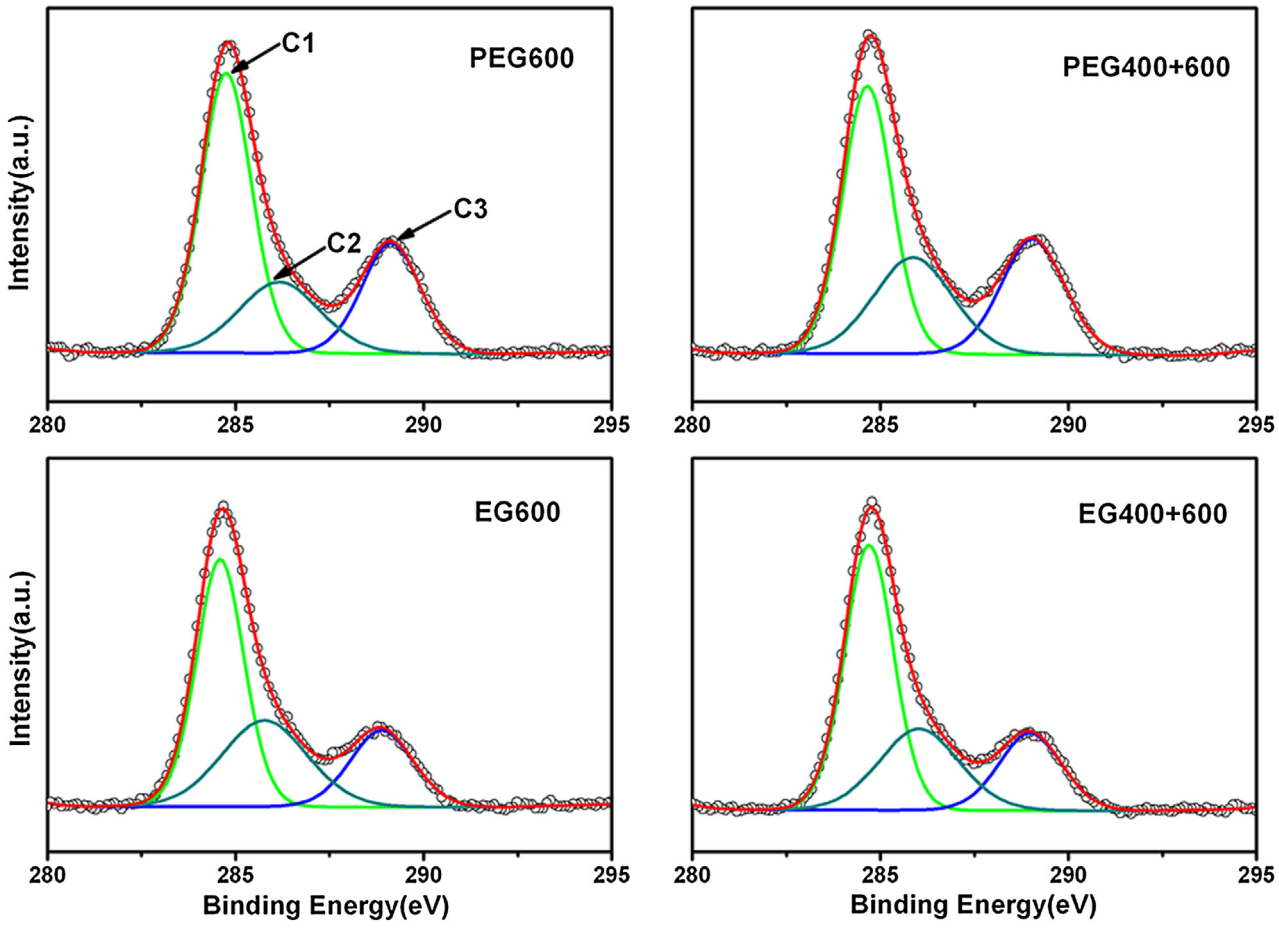

Fig. 10. The C1s XPS for different $LaFeO_{3-\delta}$ nanoparticles.

PEG400+600 (0.32). On the whole, the enhancement of sensitivity for PEG400+600 is also related with its higher Fe/La.

However, the sensitivity of EG600 to 500 ppm ethanol and above is lower than that of PEG600, while the atomic ratio of Fe/La for EG600 (0.51) is higher than 0.40 for PEG600. The abnormal is ascribed to the special layered porous structure with large area for EG600 revealed by TEM, which disfavors the adsorption of ethanol on the surface of particles. Therefore, the best sensing performance to ethanol obtained by EG400+600 is ascribed to its uniformly-sized and well-dispersed particles as well as high atomic ratio of Fe/La on the surface of particles.

Fig. 11 shows the dynamic response of resistance to 200 ppm ethanol for EG400+600 at 112 °C during one whole measuring procedure of sensitivity. When ethanol gas was introduced, the following reactions may happen:

$$(a): C_2H_5OH + 6O^{n-}{}_{(ads)} \rightarrow 2CO_2 + 3H_2O + 6ne^-$$

$$(b): C_2H_5OH + 6O^-{}_{(native)} \rightarrow 2CO_2 + 3H_2O + 6e^-$$

The electrons trapped by the adsorbed oxygen species from air and native active oxygen $O^-{}_{(native)}$ were released to semiconductor, leading to a decrease of holes, thus an increase in resistance of semiconductor sensor [20]. When the ethanol gas was taken out, oxygen from air adsorbed on the surface of $LaFeO_{3-\delta}$ and captured electrons from $LaFeO_{3-\delta}$, leading to an increase of hole and recovery of resistance towards its initial state. However, the resistance of the sensor at 112 °C after gas was taken out was somehow higher than the resistance at 112 °C before gas was set in, similar phenomenon occurred for the other measurements between 96 and 200 °C. If subsequent measurement of sensitivity was carried out afterwards, the resistance in the dry air for the calculation of sensitivity would be different. It is supposed that the ethanol gas can adsorb and release electrons to the surface of $LaFeO_{3-\delta}$ pre-adsorbed with high concentration of oxygen as the case of CO_2 [28]. The residual adsorbed ethanol would lead to the increase of resistance after gas was taken out. While perfect recovery of resistance was observed at 220 °C, indicative of complete desorption of ethanol gas. Therefore, the gas

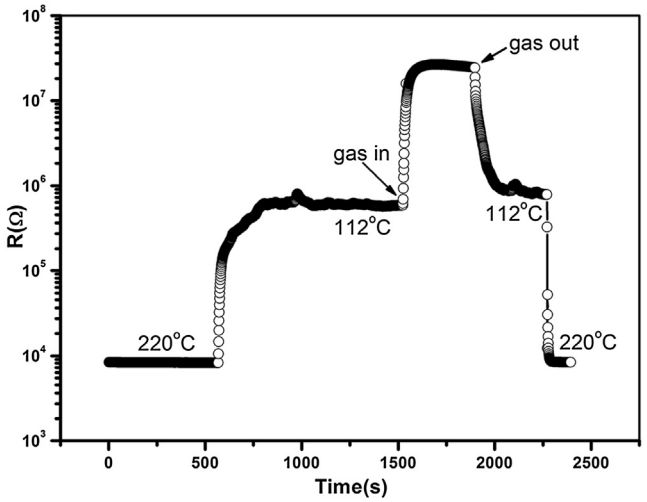

Fig. 11. Dynamic response of resistance to 200 ppm ethanol for EG400+600 at 112 °C.

desorption at 220 °C was introduced into each measuring procedure of sensitivity to make the measurement of sensitivity more precisely.

4. Conclusions

In the present work, we experimentally investigated the effect of raw material choosing (EG or PEG) and calcination process on the electrical and ethanol sensing characteristics for $LaFeO_{3-\delta}$ nanoparticles by sol-gel method. Compared to the sample choosing EG as raw material or with direct calcination at 600 °C, the choosing of PEG as raw material and additional pre-calcination at 400 °C can both result in the decrease of resistance due to the reduction of activation energy Ea, which makes the hopping of small polarons much easier. Temperature dependence of sensitivity suggests 112 °C to be the prime working temperature for these sensors. The best sensitivity to 200 ppm ethanol at 112 °C is 46.1 obtained by the sample choosing EG as raw material with additional pre-calcination, which is ascribed to its uniformly-sized and well-dispersed particles as well as high atomic ratio of Fe/La on the surface of particles. Our work demonstrates that the choosing of EG as raw material and additional pre-calcination process during citric sol-gel method is benificial for the improvement of sensing performance for $LaFeO_{3-\delta}$ nanoparticles.

Acknowledgments

This work was supported by National Natural Science Foundation of China (11404236 and 51205273) and Natural Science Foundation of Shanxi (2014021018-2 and 2015021097).

References

[1] L. Zhang, H. Qin, P. Song, J. Hu, M. Jiang, Electrical properties and acetone sensing characteristics of $La_{1-x}Pb_xFeO_3$ perovskite system, Mater. Chem. Phys. 98 (2006) 358–362.
[2] X. Liu, B. Cheng, H. Qin, P. Song, S. Huang, R. Zhang, J. Hu, M. Jiang, Preparation, electrical and gas-sensing properties of perovskite-type $La_{1-x}Mg_xFeO_3$ semiconductor materials, J. Phys. Chem. Solids 68 (2007) 511–515.
[3] X. Liu, B. Cheng, J. Hu, H. Qin, M. Jiang, Semiconducting gas sensor for ethanol based on $LaMg_xFe_{1-x}O_3$ nanocrystals, Sens. Actuators B 129 (2008) 53–58.
[4] Y.G. Cho, K.H. Choi, Y.R. Kim, J.S. Jung, S.H. Lee, Characterization and catalytic properties of surface La-rich $LaFeO_3$ perovskite, Bull. Korean Chem. Soc. 30 (2009) 1368–1372.
[5] L.H. Sun, H.W. Qin, K.Y. Wang, M. Zhao, J.F. Hu, Structure and electrical properties of nanocrystalline $La_{1-x}Ba_xFeO_3$ for gas sensing application, Mater. Chem. Phys. 125 (2011) 305–308.
[6] C.H. Feng, S.P. Ruan, J.J. Li, B. Zou, J.Y. Luo, W.Y. Chen, W. Dong, F.Q. Wu, Ethanol sensing properties of $LaCo_xFe_{1-x}O_3$ nanoparticles: effects of calcination temperature, co-doping, and carbon nanotube-treatment, Sens. Actuators B 155 (2011) 232–238.
[7] C. Doroftei, P.D. Popa, F. Iacomi, Synthesis of nanocrystalline La–Pb–Fe–O perovskite and methanol-sensing characteristics, Sens. Actuators B 161 (2012) 977–981.
[8] K. Fan, H. Qin, L. Wang, L. Ju, J. Hu, CO_2 gas sensors based on $La_{1-x}Sr_xFeO_3$ nanocrystalline powders, Sens. Actuators B 177 (2013) 265–269.
[9] P.J. Yao, J. Wang, W.L. Chu, Y.W. Hao, Preparation and characterization of $La_{1-x}Sr_xFeO_3$ materials and their formaldehyde gas-sensing properties, J. Mater. Sci. 48 (2013) 441–450.
[10] C. Shi, H. Qin, M. Zhao, X. Wang, L. Li, J. Hu, Investigation on electrical transport, CO sensing characteristics and mechanism for nanocrystalline $La_{1-x}Ca_xFeO_3$ sensors, Sens. Actuators B 190 (2014) 25–31.
[11] A. Benali, S. Azizi, M. Bejar, E. Dhahri, M.F.P. Graça, Structural, electrical and ethanol sensing properties of double-doping $LaFeO_3$ perovskite oxides, Ceram. Int. 40 (2014) 14367–14373.
[12] P. Song, H. Zhang, D. Han, J. Li, Z. Yang, Q. Wang, Preparation of biomorphic porous $LaFeO_3$ by sorghum straw biotemplate method and its acetone sensing properties, Sens. Actuators B 196 (2014) 140–146.
[13] H. Zhang, P. Song, D. Han, Q. Wang, Synthesis and formaldehyde sensing performance of $LaFeO_3$ hollow nanospheres, Phys. E 63 (2014) 21–26.
[14] H.X. Xiao, C. Xue, P. Song, J. Li, Q. Wang, Preparation of porous $LaFeO_3$ microspheres and their gas-sensing property, Appl. Surf. Sci. 337 (2015) 65–71.
[15] J. Qin, Z.D. Cui, X.J. Yang, S.L. Zhu, Z.Y. Li, Y.Q. Liang, Synthesis of three-dimensionally ordered macroporous $LaFeO_3$ with enhanced methanol gas sensing properties, Sens. Actuators B 209 (2015) 706–713.
[16] J. Qin, Z.D. Cui, X.J. Yang, S.L. Zhu, Z.Y. Li, Y.Q. Liang, Three-dimensionally ordered macroporous $La_{1-x}Mg_xFeO_3$ as high performance gas sensor to methanol, J. Alloys Compd. 635 (2015) 194–202.
[17] Y. Zhang, B. Jiang, M.J. Yuan, P.W. Li, W. Li, X.J. Zheng, Formaldehyde-sensing properties of $LaFeO_3$ particles synthesized by citrate sol–gel method, J. Sol-Gel Sci. Technol. 79 (2016) 167–175.
[18] P.A. Murade, V.S. Sangawar, G.N. Chaudhari, V.D. Kapse, A.U. Bajpeyee, Acetone gas-sensing performance of Sr-doped nanostructured $LaFeO_3$ semiconductor prepared by citrate sol–gel route, Curr. Appl. Phys. 11 (2011) 451–456.
[19] Y. Chen, H. Qin, X. Wang, L. Li, J. Hu, Acetone sensing properties and mechanism of nano-$LaFeO_3$ thick-films, Sens. Actuators B 235 (2016) 56–66.
[20] K. Cao, E.S. Cao, Y.J. Zhang, W.T. Hao, L. Sun, H. Peng, The influence of nonstoichiometry on electrical transport and ethanol sensing characteristics for nanocrystalline $LaFe_xO_{3-\delta}$ sensors, Sens. Actuators B 230 (2016) 592–599.
[21] Y. Qiu, Y.S. Luo, Z.J. Zou, Z.M. Tian, S.L. Yuan, Y. Xi, L.Z. Huang, Size effect on magnetic and dielectric properties in nanocrystalline $LaFeO_3$, J. Mater. Sci.: Mater. Electron. 25.2 (2014) 760–764.
[22] S. Phokha, S. Pinitsoontorn, S. Maensiri, S. Rujirawat, Structure, optical and magnetic properties of $LaFeO_3$ nanoparticles prepared by polymerized complex method, J. Sol-Gel Sci. Technol. 71 (2014) 333–341.
[23] X. Li, H. Zhang, F. Chi, S. Li, B. Xu, M. Zhao, Synthesis of nanocrystalline composite oxides $La_{1-x}Sr_xFe_{1-y}Co_yO_3$ with the perovskite structure using polyethylene glycol-gel method, Mater. Sci. Eng. B 18 (1993) 209–213.
[24] J.M. De Teresa, K. Dörr, K.H. Müller, L. Schultz, Strong influence of the Mn3+ content on the binding energy of the lattice polarons in manganese perovskites, Phys. Rev. B 58 (1998) R5928–R5931.
[25] G.J. Snyder, R. Hiskes, S. DiCarolis, M.R. Beasley, T.H. Geballe, Intrinsic electrical transport and magnetic properties of $La_{0.67}Ca_{0.33}MnO_3$ and $La_{0.67}Sr_{0.33}MnO_3$ MOCVD thin film and bulk material, Phys. Rev. B 53 (1996) 14434–14444.
[26] X.D. Zhou, Q. Cai, J. Yang, M. Kim, W.B. Yelon, W.J. James, Y.W. Shin, B.J. Scarfinio, H. Anderson, Coupled electrical and magnetic properties in (La, Sr)$FeO_{3-\delta}$, J. Appl. Phys. 97 (2005) 10C314.
[27] X. Liu, J. Hu, B. Cheng, H. Qin, M. Zhao, C. Yang, First-principles study of O_2 adsorption on the $LaFeO_3$ (010) surface, Sens. Actuators B 139 (2009) 520–526.
[28] X. Wang, H. Qin, L. Sun, J. Hu, CO_2 sensing properties and mechanism of nanocrystalline $LaFeO_3$ sensor, Sens. Actuators B 188 (2013) 965–971.